JOURNAL OF MATERIALS SCIENCE 27 (1992) 1785–1794

Structural studies of glassy and crystalline selenium–sulphur compounds

M. F. KOTKATA*, S. A. NOUH*
Central Research Institute for Physics, PO Box 49, H-1525 Budapest, Hungary
L. FARKAS
Research Institute for Aluminium Industry, H-1389 Budapest, Hungary
M. M. RADWAN
Physics Department, Military Technical College, Cairo, Egypt

X-ray diffraction studies revealed that the compositional dependence of the glassy structure of the binary selenium–sulphur system conforms to and can be explained by structure variations in corresponding crystalline compounds. For up to ~28% S, sulphur atoms are accommodated in the structure based on the selenium matrix and distorting it. As the percentage of sulphur reaches 50%, complete phase transitions take place. The discontinuity observed in the lattice parameters of crystalline selenium–sulphur compounds is interpreted in terms of the inter-atomic and inter-molecular forces. The crystallization process of the sample SSe_{20} was studied, where sulphur clusters were likely to be formed during the growth of selenium crystals, but sulphur atoms were accommodated in the fully crystalline selenium matrix so that no sulphur phase was formed.

1. Introduction

Because of lack of translational regularity in non-crystalline materials, it is not possible to determine its structure using a well established technique similar to that offered by Bragg's equation for crystalline materials. However, this lack of translational regularity makes it possible to change continuously the elemental ratios in non-crystalline compounds allowing systematic compositional studies to be made of them. The studies may be exploited, in most cases, to draw a structural picture in a coherent fashion.

Selenium and sulphur are miscible in all proportions [1]. A theory of equilibrium between chains and rings for liquid selenium, similar for liquid sulphur, has been developed by Eisenberg and Tobolsky [2]. Sulphur melts at approximately 391 K, and forms a liquid of relatively low viscosity, $\eta \sim 0.01$ P. This liquid is made up solely of S_8 ring molecules, as verified by vibrational spectroscopy [3]. For temperatures upto about 430 K, η remains low, but for $T > 435$ K, η rises abruptly due to the appearance of a long-chain polymer component. The maximum viscosity occurs at about 450 K, $\eta \sim 10^3$ P, and for higher temperatures, η again decreases. In contrast, trigonal selenium melts at about 490 K, and the resultant liquid has a relatively high viscosity, ~ 30 P. The viscosity of liquid selenium also decreases with increasing temperature, and is about an order of magnitude smaller than that of sulphur over the temperature range ~ 400–800 K [4].

If local valence requirements are to be satisfied in the alloys Se–S, then any structural groupings other than rings or chains would appear to be excluded [5]. Raman studies by Ward and others suggested the formation of mixed eight-membered rings, possibly Se_3S_5, which increases in concentration at the expense of the Se_8 rings [3, 6, 7]. Later a model was proposed that analysed the Raman spectra by a simple molecular model of a three structural unit, rather than by Ward's mixed ring model [8].

In a previous paper [9], the homogeneous glass-forming region for air-quenched melts (350 °C, 2 h) in the binary system Se–S was reported, together with metastable melt crystallization temperatures and differential thermal analysis (DTA) data. In addition, the compositional dependence of the non-isothermal crystallization kinetic parameters for Se–S glasses were studied and discussed. The nature of the growth phases during both the amorphous–crystal and liquid–crystal transition of a binary compound, namely SSe_{20}, have also been discussed and compared to that of pure-selenium [10]. The photo-effect on crystallization kinetics of amorphous selenium doped with sulphur has been reported [11], as has the compositional dependence of the photoconductivity gap for different Se–S glasses [12].

In the present work, results obtained from X-ray diffraction (XRD) patterns and the effect of change in composition on both glassy and crystalline structures for Se–S compounds are discussed. The process of

* *Permanent address*: Physics Department, Faculty of Science, Ain Shams University, Cairo, Egypt.

0022–2461

crystallization and the rate of crystal growth for the compound SSe_{20} was studied by analysing XRD patterns from isothermally treated samples between the glass transition, T_g, and crystallization, T_c temperatures for different periods of time.

2. Experimental procedure

A series of Se–S compounds of compositions covering the whole range of proportions between selenium and sulphur was prepared from high purity (99.999%) selenium and sulphur by heating mixtures of the elements in vacuum-sealed (10^{-6} mm Hg) Pyrex tubes in the following temperature steps: first the mixtures were heated to 140 °C and kept at this temperature for 1 h; then heated to 230 °C and kept for 1 h; then the furnace temperature was increased to 300 °C and synthesis was continued for 2 h, during which the molten

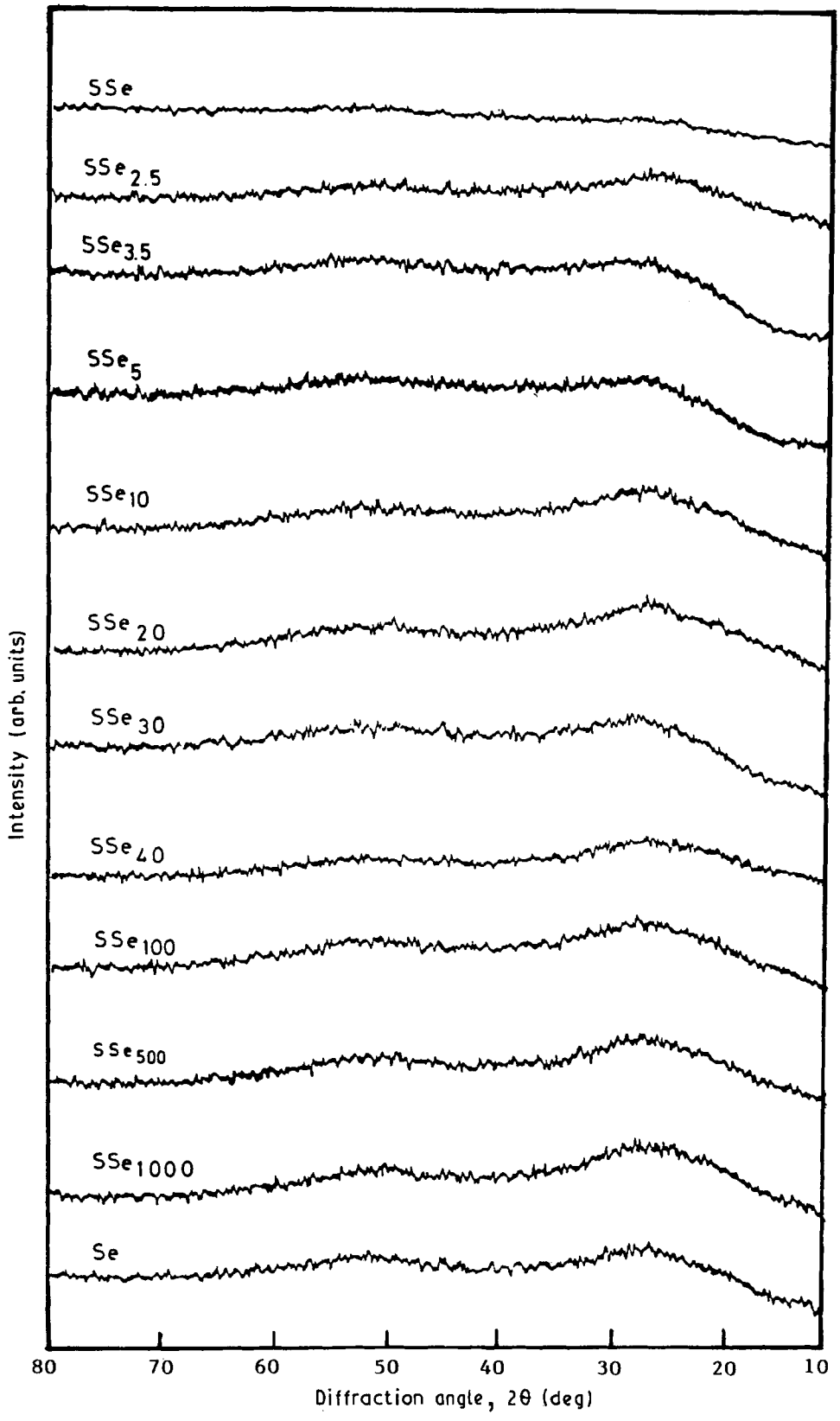

Figure 1 XRD patterns of Se–S quenched samples with ≤ 50 at % S.

solution was occasionally shaken vigorously. The molten masses (5 g) were quenched in iced-water. The quenched ingots of the Se–S compounds were found to be glassy or crystalline depending on the percentage of sulphur content as indicated by XRD and differential thermal analysis (DTA) measurements. The results are found to be in good agreement with those previously obtained [9].

The polycrystalline forms of the resulting glassy compounds were affected by annealing in the range of their softening and crystallization temperatures, T_g–T_c [13]. The structure of the crystalline state was investigated to explain structural features of glassy compounds. The samples were ground in an agate morter.

The XRD measurements were made with a Philips powder diffractometer, equipped with a grafite mono-

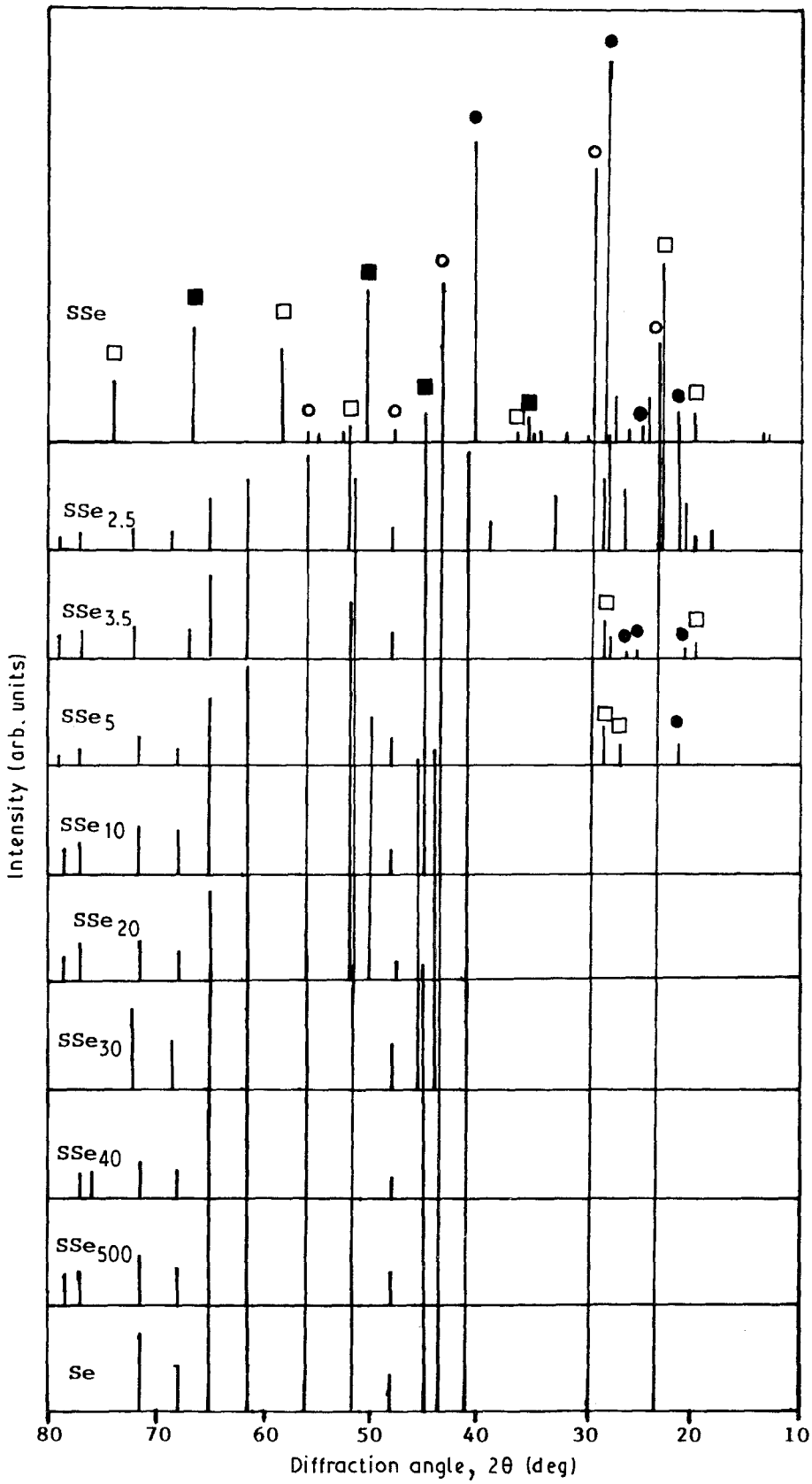

Figure 2 XRD patterns of Se–S crystallized samples for compositions with $\leqslant$ 50 at % S. (○) Se, (●) S, (□) SeS, (■) $S_{0.56}Se_{0.44}$.

TABLE I Interplanar spacings and relative intensities of crystallized Se–S samples with up to 50 at % S

hkl	Se			SSe_{500}			SSe_{40}			SSe_{30}			SSe_{20}		
	d_{obs} (nm)	d_{cal} (nm)	(I/I_o) (%)	d_{obs} (nm)	d_{cal} (nm)	(I/I_o) (%)	d_{obs} (nm)	d_{cal} (nm)	(I/I_o) (%)	d_{obs} (nm)	d_{cal} (nm)	(I/I_o) (%)	d_{obs} (nm)	d_{cal} (nm)	(I/I_o) (%)
100	0.378 54	0.378 32	93	0.378 79	0.378 07	83	0.378 69	0.378 34	84	0.378 71	0.378 65	86	0.379 69	0.379 22	75
101	0.300 54	0.300 62	100	0.300 83	0.300 53	100	0.300 49	0.300 51	100	0.300 72	0.300 60	100	0.300 31	0.300 66	100
110	0.218 58	0.218 43	97	0.218 20	0.218 28	58	0.218 54	0.218 43	53	0.218 55	0.218 61	71	0.218 83	0.218 94	56
102	0.207 10	0.207 16	95	0.206 95	0.207 17	90	0.207 04	0.207 01	89	0.206 88	0.206 97	90	0.206 63	0.206 77	74
111	0.199 80	0.199 85	90	0.199 64	0.199 75	88	0.199 78	0.199 82	60	0.199 76	0.199 93	88	0.200 11	0.200 12	71
200	0.189 01	0.189 16	10	0.188 86	0.189 04	8	0.189 09	0.189 17	6	0.189 34	0.189 32	11	0.189 67	0.189 61	7
201	0.176 57	0.176 71	87	0.176 56	0.176 61	71	0.176 70	0.176 69	56	0.176 89	0.176 80	87	0.176 95	0.176 99	62
201															
003	0.165 04	0.165 05	60												
112	0.163 68	0.163 79	60	0.163 85	0.163 75	38	0.163 74	0.163 72	40	0.163 76	0.163 75	74	0.163 86	0.163 75	49
103	0.151 30	0.1528	53												
202	0.150 35	0.150 31	53	0.150 33	0.150 27	31	0.150 35	0.150 26	31	0.150 33	0.150 30	64	0.150 37	0.150 33	38
210	0.143 00	0.142 99	43	0.142 85	0.142 90	27	0.143 30		23	0.143 10	0.143 11	43	0.143 34	0.143 33	25
211	0.137 43	0.137 38	14	0.137 38	0.137 30	10	0.137 35	0.137 37	7	0.136 80		14	0.137 61	0.137 64	8
113	0.131 71	0.131 69	23	0.131 66	0.131 68	13	0.131 57	0.131 60	10	0.130 87		21	0.131 47	0.131 49	12
203				0.123 85		8	0.123 23		7				0.123 85		9
301				0.121 86		8	0.121 85		6				0.121 86		7

TABLE I Continued.

SSe_{10}			SSe_5			$SSe_{3.5}$			$SSe_{2.5}$			SSe		
d_{obs} (nm)	d_{cal} (nm)	(I/I_o) (%)	d_{obs} (nm)	d_{cal} (nm)	(I/I_o) (%)	d_{obs} (nm)	d_{cal} (nm)	(I/I_o) (%)	d_{obs} (nm)	d_{cal} (nm)	(I/I_o) (%)	d_{obs} (nm)	d_{cal} (nm)	(I/I_o) (%)
												0.655 96		1
												0.632 64		2
									0.467 14		4			
						0.444 00		3				0.444 00		7
									0.433 28		3			
						0.422 50		3	0.423 08		12			
			0.410 90		9									
									0.405 40		36			
0.378 71	0.379 23	79	0.377 80	0.378 82	75	0.378 49	0.379 20	84	0.378 71	0.378 48	77	0.378 60		26
												0.360 48		11
												0.355 80		4
						0.348 90		2						
			0.333 50		5	0.336 39		1	0.336 39		17	0.331 48		3
												0.324 38		11
						0.318 70		5	0.317 59		31			
			0.312 30		5.2	0.313 22		10	0.313 22		18	0.311 08		100
0.300 35	0.300 53	100	0.300 52	0.300 46	100	0.300 55	0.300 65	100	0.300 69	0.300 76	100	0.299 50		1
												0.279 72		2
									0.271 38		13			
												0.260 36		3
												0.256 40		1
												0.251 53		5
												0.243 62		2
									0.236 50		7			
												0.221 19		79
0.218 92	0.218 95	53	0.218 72	0.218 71	32	0.218 95	0.218 93	39	0.218 59	0.218 51	26			
0.206 60	0.206 60	64	0.206 58	0.206 71	65	0.206 82	0.206 78	77	0.206 90		70			
0.200 08	0.200 08	63	0.199 84	0.199 94	49	0.200 10	0.200 11	62	0.199 82	0.199 93	35	0.200 40		2
0.189 50	0.189 61	7	0.189 34	0.189 34	5	0.189 65	0.189 60	6	0.189 56		5	0.189 56		2
												0.180 74		40
0.177 00	0.176 96	58	0.176 86	0.176 83	10	0.177 01	0.176 98	48	0.176 76	0.176 78	16			
			0.175 70		43				0.175 70		33	0.173 64		3
												0.166 56		1
0.164 07	0.164 24	51	0.163 75	0.163 65	30	0.163 80		35	0.163 81	0.163 87	25	0.164 22		1
												0.156 81		24
0.150 73	0.150 72	38	0.150 29	0.150 23	25	0.150 32	0.150 33	30	0.150 44	0.150 38	19			
0.143 32	0.143 33	30	0.143 10	0.143 18	17	0.143 35	0.143 32	22	0.143 30		14			
												0.140 25		31
0.137 63	0.137 63	10	0.137 57	0.137 51	5	0.137 59	0.137 63	7	0.136 80		4			
0.131 47	0.131 39	13	0.131 40	0.131 44	8	0.131 17		9	0.131 17		6			
												0.128 11		16
0.123 85		9	0.123 85		5	0.123 85		7	0.123 85		4			
0.121 86		8	0.121 21		4	0.121 21		6	0.121 21		3			

chromator crystal. The copper radiation was generated by 45 kV accelerating voltage and 30 mA anode current. The patterns were recorded with a scanning speed of 1° or 2° (2θ) min^{-1}. High-purity KCl was used as internal standard to correct the systematic error in the line positions. A second-order curve was determined in order to calculate the necessary shift to be applied at different 2θ values for correcting the measured line positions.

3. Results and discussion

3.1. The glassy state

It was possible to prepare bulk glassy alloys for the Se–S system only up to 50% sulphur content. XRD patterns obtained from 12 glassy samples of the binary system Se–S, which starts with pure selenium and goes up to the composition SeS, are shown in Fig. 1. The XRD pattern for pure selenium is characterized by the two humps extending in the range of 2θ 18°–34° (0.493–0.264 nm d-spacing) and 44°–62° (0.201–0.150 nm). The radial distribution function for this diffraction pattern results in a number of nearest neighbours ($Z = 2$) and a radius of the first coordination sphere (~ 0.23 nm) which are practically the same as those resulting from either of the two crystalline forms of monoclinic and trigonal selenium [5]. The addition of small percentage of sulphur to the selenium results in minor changes in the shape of the diffraction pattern, indicated by small shifts in the hump positions and their relative intensities. This shows that the proposed structure of amorphous selenium (chain-like morphology, possibly containing ring molecules) is not destroyed by the addition of up to 28 at % S. Possibly, sulphur atoms are accommodated in the selenium matrix resulting in some local disorders. However, addition of sulphur results in distortion of the selenium morphology which is monotonic with increasing sulphur content, as is clear by the changes in the second hump, which nearly disappears as the percentage of sulphur reaches about 17%. As the sulphur content increases to 50%, a complete change of the shape of the diffraction pattern is observed which indicates complete destruction of the selenium morphology, and that a structural phase transition rather than some local disorder did take place. These observed changes of the structure of the Se–S glassy binary system, while increasing the sulphur percentage are in complete conformation with those observed in the crystal structure of the same compositions described later.

3.2. The crystalline state

XRD peaks for ten crystallized samples having compositions from pure selenium up to 50% sulphur-alloyed selenium, obtained by proper annealing of the as-prepared glassy state, are shown in Fig. 2. For samples of pure selenium to ~ 9 at % S, all the peaks can be indexed based on trigonal selenium (ASTM Card no. 6-0362). For higher percentages of sulphur, additional peaks could be observed indicating the presence of additional phases which could be identified as selenium sulphide (ASTM Card no. 2-0320) and some lines of sulphur could be detected.

As the atomic percentage of sulphur is increased to 50%, a new phase, namely sulphur–selenium (ASTM Card no. 20-1229) is present together with the previously formed phases of SeS and sulphur. At this concentration of sulphur, the trigonal selenium phase has completely disappeared.

For sulphur percentages up to nearly 28%, the effect of the sulphur on the crystal structure of selenium was indicated by small changes in the positions of the selenium peaks, which resulted from the variation of the hexagonal lattice parameters. The variations of the lattice parameters were determined from the measured d-values by a least squares refinement of the unit cell using a modified IBM PC/AT version of the program PIRUM, originally written by Werner [14].

Table I contains the diffraction lines used in the

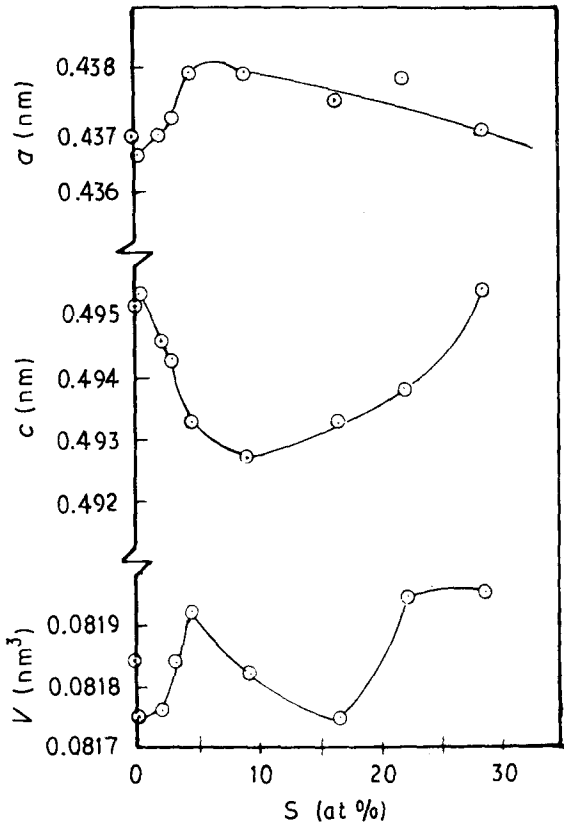

Figure 3 The compositional dependence of lattice parameters and unit cell volume of Se–S compounds.

TABLE II Unit cell parameters and volume of Se–S compounds

Composition	S (at %)	Lattice parameters		Unit cell volume
		a (nm)	c (nm)	(nm^3)
Se	0.0	0.4369	0.4952	0.081 84
SSe_{500}	0.199	0.4366	0.4953	0.081 75
SSe_{40}	2.44	0.4369	0.4946	0.081 76
SSe_{30}	3.23	0.4372	0.4943	0.081 84
SSe_{20}	4.76	0.4379	0.4933	0.081 92
SSe_{10}	9.09	0.4379	0.4927	0.081 82
SSe_{5}	16.67	0.4374	0.4933	0.081 75
$SSe_{3.5}$	22.22	0.4378	0.4938	0.081 94
$SSe_{2.5}$	28.57	0.4370	0.4954	0.081 95

refinement and Table II gives the refined cell parameters and unit cell volumes. These cell parameters are also shown in Fig. 3, from which one can see that with the increase of atomic per cent sulphur (up to 9%) the a-value increases from 0.4369 nm (for pure selenium) to 0.4379 nm, while the c-value decreases (0.4952–0.4927 nm). For higher percentages of sulphur, a reverse behaviour takes place. This behaviour can be explained when considering the proposed selenium chain-like morphology, possibly containing ring molecules, in which entangled chain molecules are held together with weak intermolecular forces, mostly consisting of the Van der Waals type. The primary decrease in the c-value is mainly due to an increase in the Van der Waals force with a small addition of sulphur atoms. For higher percentages of sulphur (> 5 at %), the higher values of single-bond energies of S–S bonds and S–Se bonds (2.2 and 2.05 eV, [15]) relative to the Se–Se bond energy (1.9 eV, [15]) would result in chain contraction, leading to the observed decrease in the a-value. Chain contraction resulting from the addition of sulphur to selenium has been theoretically expected before, during analysis based on the equilibrium liquid phase [5].

From the results of the X-ray measurements, the conclusion can be drawn that a small amount of sulphur (up to about 28 at %) can be built in the selenium lattice making the described changes in the lattice parameters and the unit cell volumes. For higher percentages of sulphur up to 50%, the selenium matrix is completely destroyed and new phases are formed.

XRD scans from an additional four samples completing the whole range of Se–S compositions for sulphur percentages ranging from > 50 at % up to pure sulphur, are shown in Fig. 4. The figure shows the characteristic diffraction lines for each of these four compositions. It is worth mentioning that these compositions were found to be in the crystalline state when prepared by the quenching technique. The interplanar spacing (d-values) and relative intersities (I/I_0) of these four compositions are given in Table III. The identification of the phases present in the patterns of these compositions was not possible because of the great overlapping of peaks present.

3.3. Crystallization process

The composition SSe_{20} (4.76 at % S) was selected to study the process of crystallization and the rate of crystal growth by subjecting the supercooled (as-prepared) sample to an isothermal treatment between its T_g (43 °C) and T_c (101 °C at 10 °C min^{-1}) temperatures, namely 80 °C, for different periods of time.

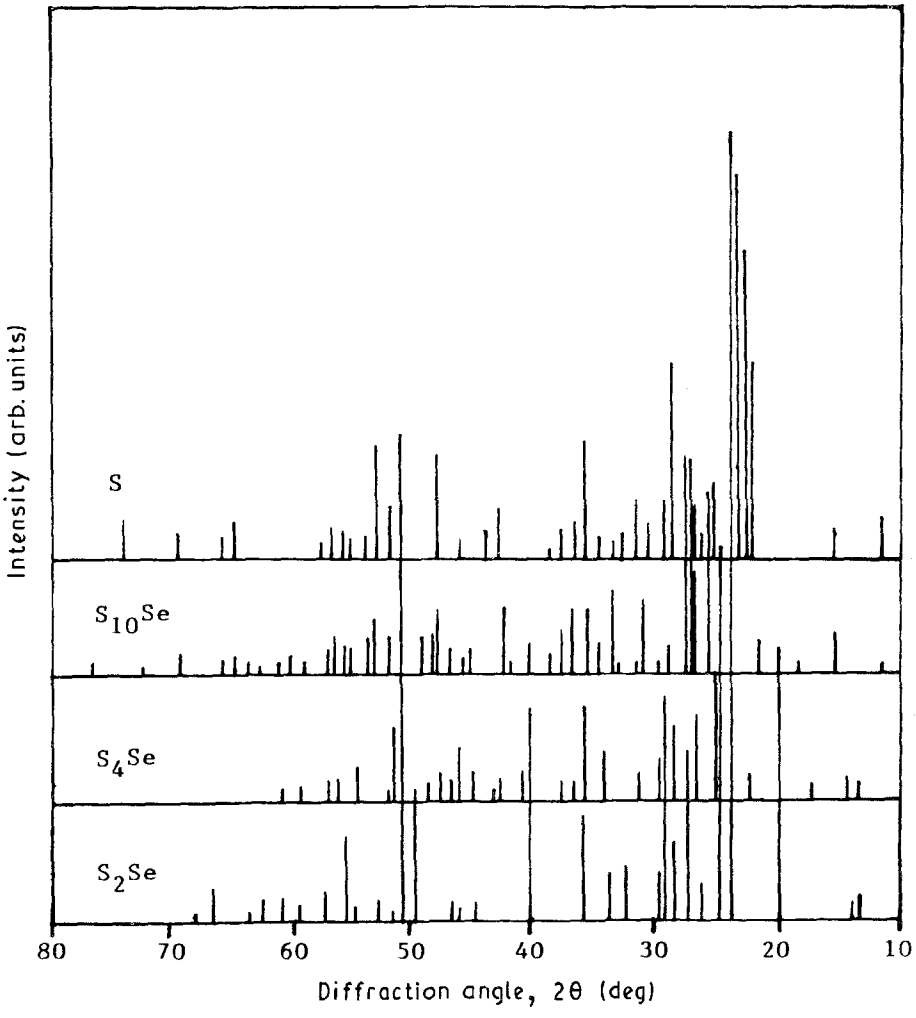

Figure 4 XRD patterns of Se–S crystalline samples for compositions with > 50 at % S.

TABLE III Interplanar spacings and relative intensities of crystalline Se–S samples with > 50 at % S

S_2Se		S_4Se		$S_{10}Se$		S	
d (nm)	I/I_o (%)	*d* (nm)	I/I_o (%)	*d* (nm)	I/I_o (%)	*d* (nm)	I/I_o (%)
				0.756 44	3	0.750 05	9
				0.5747	12	0.560 95	8
				0.4054	11	0.402 26	46
		0.388 39	6	0.381 33	100	0.3862	90
0.368 26	48	0.369 01	100	0.367 96	77	0.373 39	100
				0.3558	9	0.3558	3
0.349 62	58	0.345 88	30	0.3443	40	0.3443	17
						0.342 74	16
0.331 72	8			0.3335	28	0.336 39	6
		0.327 06	22	0.3211	53	0.326 71	15
0.317 37	40	0.315 61	41	0.3102	30	0.318 70	27
0.307 31	18	0.3075	18			0.3075	45
0.301 63	10	0.3007	23	0.300 93	7	0.3008	12
0.295 20	11	0.294 25	8	0.294 25	4	0.287 60	7
				0.2841	18	0.278 53	14
0.273 24	13	0.274 87	5	0.276 02	3	0.271 46	6
0.260 36	12			0.2619	18	0.263 71	3
		0.258 69	12	0.2564	7	0.2564	4
0.249 50	25	0.2485	20	0.2485	15	0.2485	28
		0.2420	5	0.2420	17	0.2420	9
		0.2365	3	0.2365	12	0.2365	5
		0.233 27	2	0.2284	5	0.230 97	2
		0.210 13	4	0.2108	18	0.210 37	10
		0.206 71	3			0.2056	6
0.199 58	5	0.198 34	7	0.198 47	6	0.201 47	3
0.193 74	4	0.193 94	13	0.195 71	4	0.195 32	4
0.190 30	6	0.189 52	6	0.1897	16	0.189 56	23
0.178 63	100	0.178 57	22	0.1782	12	0.178 57	42
		0.177 40	15	0.175 31	8	0.1757	12
0.174 32	3	0.173 46	2	0.1724	14	0.1724	26
0.170 15	6	0.168 36	8	0.1696	8	0.1696	5
0.165 95	5			0.1662	5	0.1646	4
0.164 44	20	0.164 15	6	0.1646	8	0.164 23	6
0.161 53	7	0.161 27	4	0.1619	10	0.1614	8
				0.1603	7	0.159 03	3
				0.1436	4	0.1433	7
				0.1421	3	0.141 56	5
				0.135 74	4	0.134 59	4
						0.128 11	8

TABLE IV X-ray intensity, I (arb. units) and interplanar spacing d for different isothermal crystallization of glassy SSe_{20} at 80 °C

10 min		20 min		30 min		35 min		40 min		45 min		90 min		120 min		150 min		Crystalline		hkl
d (nm)	I	d (nm)	I	d (nm)	I	d (nm)	I	d (nm)	I	d (nm)	I	d (nm)	I	d (nm)	I	d (nm)	I	d (nm)	I	
										0.410 93	0.7									1 1 5
												0.381 32	5	0.381 32	3	0.381 32	3.0	0.379 69	42	1 0 0
		0.376 54	0.5	0.376 54	0.7	0.376 54	0.7	0.376 54	3	0.376 54	3.0									2 2 2
										0.339 73	0.7									2 2 4
0.301 34	0.8	0.300 84	1.0	0.301 34	2.0	0.300 84	2.0	0.299 46	10	0.299 82	9.0	0.300 84	12	0.301 44	10	0.301 44	9	0.300 31	55	1 0 1
														0.234 14	1	0.235 62	1			3 3 5
								0.217 12	1	0.217 12	1	0.219 36	1	0.219 36	1	0.219 40	1	0.218 83	30	1 1 0
																0.208 70	2			2 2 1 0
								0.206 44	3	0.206 44	2	0.207 12	3	0.207 34	2	0.207 30	2	0.206 63	41	1 0 2
								0.198 96	1	0.197 88	1	0.200 16	2	0.200 62	2	0.200 62	3	0.200 11	39	1 1 1
																		0.189 67	4	2 0 0
								0.1760	1	0.1760	1	0.176 92	2	0.176 92	2	0.1782	1	0.176 95	34	2 0 1
								0.164 02	1	0.164 02	1	0.164 02	2	0.164 02	1	0.164 02	1	0.163 86	27	1 1 2
								0.150 38	1	0.150 38	1	0.150 38	2	0.150 38	1	0.150 38	0.7	0.150 37	21	2 0 2
												0.143 12	1	0.143 12	1	0.1433	1	0.143 34	14	2 1 0
																		0.137 61	5	2 1 1
																		0.131 47	7	1 1 3
																		0.123 85	5	3 0 1
																		0.121 86	4	–

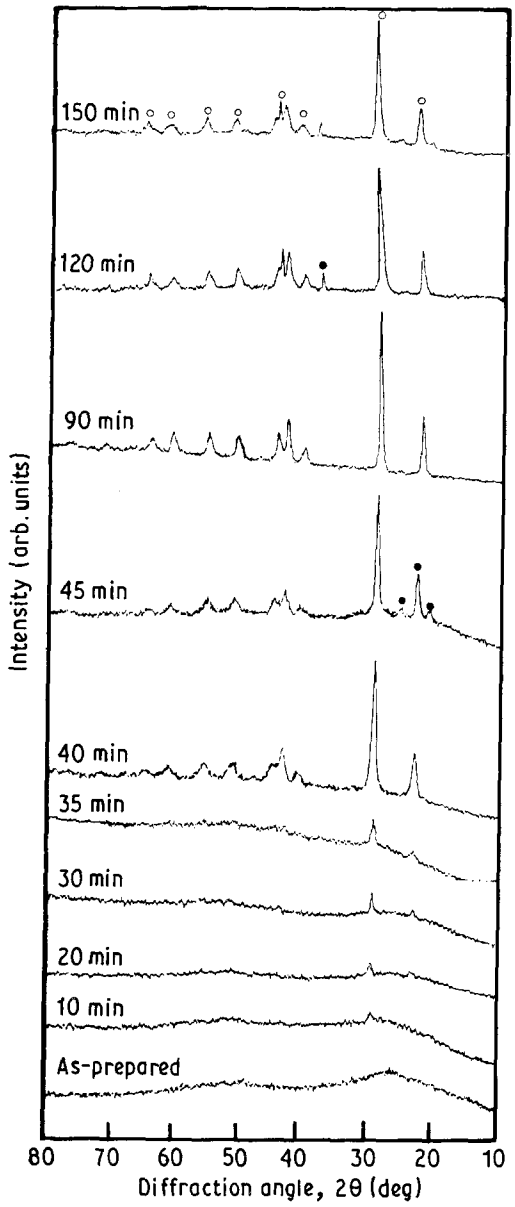

Figure 5 XRD patterns of the sample SSe_{20} annealed at 80 °C for different times. (○) Se, (●) S.

After the required time, the evacuated sealed tube containing the sample was quenched in iced-water to stop any possible phase transition. After heat treatment, an X-ray scanning covering the angular range of the two broad maxima (humps) has been recorded. Fig. 5 shows the Bragg angle dependence of diffraction line intensities of amorphous SSe_{20} crystallized at 80 °C for different soaking times. The intensity, I, and the interplanar spacings, d, were measured for all patterns and are given in Table IV along with the results for a completely crystallized SSe_{20} sample. As mentioned before, the completely crystallized sample contains only trigonal selenium phase with sulphur atoms accommodating in its matrix. However, XRD patterns for soaking times from 20–150 min contain different peaks, indicating the formation of sulphur crystalline phase in addition to the dominating selenium phase. This can be explained by the likely formation of sulphur clusters during the growth of selenium crystals. Once the selenium has been completely crystallized accommodating sulphur atoms in its matrix, it is not possible for sulphur phases to be formed. For the selenium crystal phase, the 1 0 1 line appears after 10 min soaking time. It needed 40 min soaking time for the appearance of an additional six diffraction line: $d = 0.21712$, 0.20644, 0.19896, 0.1760, 0.16402 and 0.15038 nm.

4. Conclusions

1. For the binary system Se–S, it was possible to prepare bulk to glassy samples for compositions from pure selenium alloys containing 50% S by quenching from the melt.

2. XRD from glassy samples shows a distortion in a selenium-based morphology with increasing sulphur content in the alloy. Complete destruction of this morphology happens when the sulphur content reaches 50%.

3. Structural changes in crystalline samples prepared by annealing of the corresponding glassy compositions, conform to and explain changes observed in glassy state.

4. A monotonic decrease in the c-lattice parameter with sulphur addition up to 9% is attributed to a corresponding increase in the intermolecular Van der Waals forces. A monotonic increase in the a-lattice parameter for sulphur content $> 5\%$ is explained in terms of the sulphur and selenium single bond energy.

5. In the process of crystallization of the sample SSe_{20}, sulphur clusters are likely to be formed during the growth of selenium crystals but sulphur atoms accommodate in the fully crystalline selenium matrix, so that no sulphur phase is formed.

References

1. P. M. HANSEN and K. ANDERKO, "Construction of Binary Alloys" (McGraw-Hill, New York, 1958) p. 1162.
2. A. EISENBERG and A. V. TOBOLSKY, *J. Polym. Sci.* **46** (1960) 19.
3. A. T. WARD, *J. Phys. Chem.* **72** (1968) 4133.
4. G. LUCOVSKY, "Selenium, The Amorphous and Liquid States", edited by E. Gerlach and P. Grosse (Springer-Verlag, New York, 1979) p. 178.
5. N. F. MOTT and E. A. DAVIS, "Electronic Processes in Non-Crystalline Materials" (Clarendon, Oxford, 1979) Ch. 10.
6. A. T. WARD. *J. Non-Cryst. Solids* **4** (1970) 4110.
7. J. SCHOTTMILLER, M. TABAK, G. LUCOVSKY and A. WARD, *ibid.* **4** (1970) 80.
8. A. ARAI, *ibid.* **77–78** (1985) 1355.
9. M. F. KOTKATA, M. H. EL-FOULY, A. Z. EL-BEHAY and L. A. EL-WAHAB, *Mater. Sci. Engng* **60** (1983) 163.
10. M. K. EL-MOUSLY, M. F. KOTKATA and S. A. SALAM, *J. Phys. C* **11** (1978) 1077.
11. M. F. KOTKATA, F. M. AYAD and M. K. EL-MOUSLY, *J. Non-Cryst. Solids* **33** (1979) 13.
12. M. F. KOTKATA, M. FÜSTOSS-WEGNER, L. TÓTH, G. ZENTAI and S. A. NOUH, to be published.
13. M. H. EL-FOULY, M. F. KOTKATA and S. A. NOUH, to be published.
14. P. E. WERNER, *Arkiv Kemi* **31** (1969) 513.
15. LINUS PAULING, "The Nature of the Chemical Bond", 3rd Edn (Cornell University Press, Ithaca, New York, 1960).

Received 21 November 1990
and accepted 10 April 1991